DOI: 10.21062/mft.2026.039 © 2026 Manufacturing Technology. All rights reserved. http://www.journalmt.com

Effect of 3D Printing on Changes in Modulus of Elasticity E Measured by Ultrasound, Bending Test and EBSD

Jana Vesela (0000-0002-2314-634X), Petr Beneš (0000-0001-5673-0588), David Bricín (0000-0002-9354-2751)
Research Centre Rez, 301 00 Morseova 4 Plzen, Czech Republic. E-mail: jana.vesela@cvrez.cz

The use of metal additive manufacturing is becoming an essential tool in industrial production, offering opportunities for rapid innovation and increased efficiency. It is widely applied in prototype fabrication and spare-part manufacturing, where it simplifies production processes, reduces costs, and shortens lead times. This study focuses on evaluating the influence of 3D printing parameters on the elastic modulus E measured in individual printing axes, and its change after thermomechanical post-processing using Hot Isostatic Pressing (HIP). Elastic moduli were determined non-destructively using ultrasonic testing and destructively through three-point bending tests and EBSD (Electron Backscatter Diffraction) analysis.

Keywords: ultrasound velocity, 3D printing, elastic modulus E, three-point bending test, elastic stiffness coefficient

1 Introduction

The elasticity modulus is one of the basic mechanical parameters of steel. It defines the relationship between the applied stress and the resulting deformation in the elastic range and is key for predicting deformations and ensuring the reliability of structural components. Accurate values of Young's modulus are needed when assessing the strength of structures, especially for materials produced with advanced technologies, like additive manufacturing. Several factors affect the elastic modulus of steel, including chemical composition, manufacturing technology, microstructure, and operating temperature. In this study, the values of the elasticity modulus calculated from ultrasonic measurements were verified through mechanical tests and stiffness analysis based on EBSD.

Measuring the elastic modulus using the ultrasonic method is technically simple and quick. A major advantage of UT measurement is that it can be done without needing to take a sample, so it's non-destructive. [1] On the other hand, determining the elastic modulus using three-point bending is one of the typical methods commonly used to find this modulus. The downside of this method is that it requires taking and preparing a test sample destructively, and you can't use tiny samples. The EBSD method is one of the commonly used tools in metallographic research. Being able to determine the elastic modulus with this method also significantly expands its use in the metallographic characterization of materials. [2] Due to the different physical principles of the various methods for determining the modulus of elasticity, the goal is to see what differences arise when measuring it with different techniques. Materials made using AM technologies are highly anisotropic, which of course also affects how the measurement depends on direction in relation to the modulus of elasticity. From this point of view, measuring the modulus of elasticity using UT seems very advantageous, because measuring the modulus in all directions of the material is easy and quick compared to other techniques.

2 Test samples

Material A508 was selected for evaluation in five variants. This steel is intended to form part of a graded joint together with 316L stainless steel, potentially used in piping applications.
For A508 printing, Directed Energy Deposition (DED) technology was employed, using two laser power settings (1000 and 1250 W). Powder particle sizes ranged from 50–150 μm and were atomized either in nitrogen or argon.

Table 1 summarizes the printed samples. Prior to ultrasonic testing, each printed prism was machined to flat surfaces, and measurement points were defined in all three axes, Fig. 1.

Ultrasonic properties were measured in the X, Y, and Z printing directions on samples in their as-printed state and again after HIP treatment. For comparison with ultrasonic-based elastic modulus E, additional destructive tests were conducted: three-point bending test → flexural modulus and EBSD → crystallographic elastic stiffness.

Tab. 1 *Samples description*

Sample No.	Material	Marking	Type	Dimensions [mm]	State	No. of measuring points
1	A508 (carbon steel)	1000-Ar	Atomized to Argon	34x34x60	after HIP	18/18/9 (in axis X/Y/Z)
2		1000-2	Atomized to Nitrogen			
3		1250-Ar	Atomized to Argon			
4		1250-4	Atomized to Nitrogen			
5		1250-6	Atomized to Nitrogen			

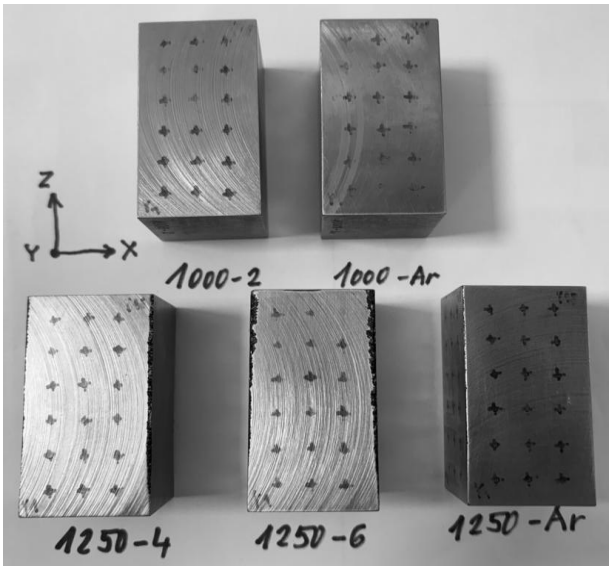


Fig. 1 *Samples of A508 with marking and axis of print*

3 Methodology of ultrasonic testing

Ultrasonic measurements were performed using the Pulse-Echo (P/E) technique. Propagation velocities of longitudinal (cL) and transverse (cT) waves were measured before and after HIP processing. These values were used to calculate Poisson's ratio (ν) and the elastic modulus E using the following equations (1) [4], [5] and (2) [4].

Poisson's number:

$$v = \frac{1 - 2(\frac{c_T}{c_L})^2}{2 - 2(\frac{c_T}{c_L})^2} \quad (1)$$

Where:

ν…Poisson's number;

c_T…Velocity of transversal waves [m/s];

c_L…Velocity of longitudinal waves [m/s].

The modulus of elasticity E [GPa]:

$$E = c_L^2 \rho \frac{(1+v)(1-2v)}{(1-v)} \quad (2)$$

Where:

ρ…Density of material [kg/m³];

c_T…Velocity of transversal waves [m/s];

c_L…Velocity of longitudinal waves [m/s];

ν…Poisson's number.

Measurements were performed using longitudinal and transverse probes with a center frequency of 5 MHz and a transducer diameter of 12.7 mm. For precise thickness calibration, 3D-scanned local thickness values were used at each measurement point. In addition, attenuation was evaluated using the second back-wall echo drop. For the above equation (2), a density datasheet value of 7850 kg/m³ was used for A508 steel.

4 Results of Ultrasonic Measurements

The speed measurements of both longitudinal and transverse waves were processed and evaluated for all axes before and after the HIP process to determine its effect on the value of the E modulus. Figures 2 and 3 demonstrate the trend along the Y axis in both states i.e. before and after HIP process for both velocities (longitudinal and transversal); similar trends were observed for the X and Z axes.

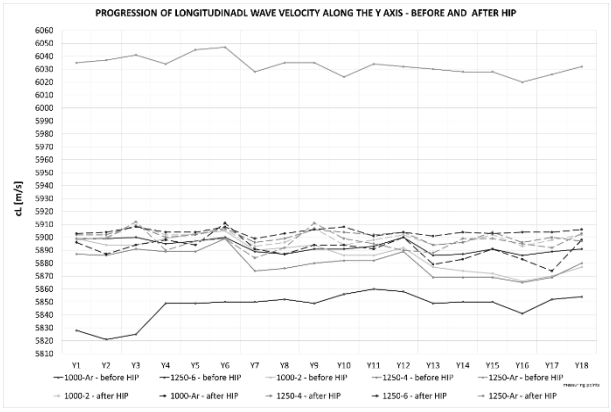


Fig. 2 *Samples of A508 - Progression of longitudinal wave velocity along the Y printing axis - before and after HIP*

Table 2 summarizes the average values of the measured ultrasound velocities of the individual samples and calculated values of Poisson's ratios, and moduli of elasticity after HIP in all three axes of printing. All values are given with the sample standard deviation.

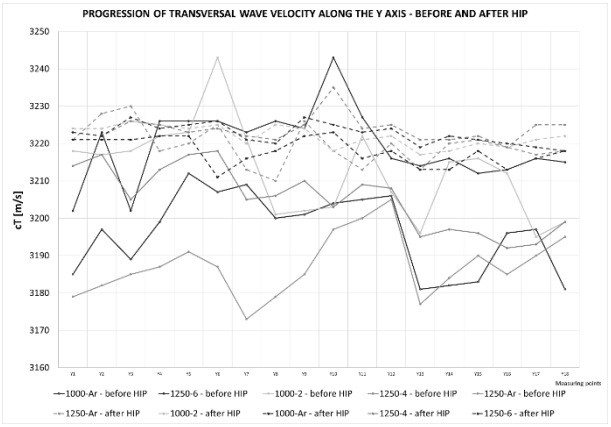


Fig. 3 *Samples of A508 - Progression of transversal wave velocity along the Y printing axis - before and after HIP*

Tab. 2 *Modulus of elasticity E measured by ultrasonic testing after HIP*

Sample No.	Direction	c_L (m/s)	c_T (m/s)	u	E (GPa)
1000-Ar	X	5896 ± 14.5	3220 ± 9.0	0.2875 ± 0.0002	150.3 ± 0.9
	Y	5891 ± 18.5	3218 ± 6.0	0.2873 ± 0.0008	150.1 ± 0.5
	Z	5890 ± 2.0	3222 ± 1.5	0.2865 ± 0.0001	150.6 ± 0.2
1000-2	X	5901 ± 12.0	3221 ± 8.5	0.2878 ± 0.0004	150.3 ± 0.8
	Y	5900 ± 8.0	3222 ± 4.5	0.2875 ± 0.0001	150.5 ± 0.4
	Z	5898 ± 2.5	3222 ± 2.0	0.2873 ± 0.0001	150.5 ± 0.2
1250-Ar	X	5894 ± 11.0	3221 ± 6.0	0.2871 ± 0.0002	150.4 ± 0.6
	Y	5897 ± 14.0	3219 ± 10.0	0.2878 ± 0.0004	150.2 ± 1.0
	Z	5892 ± 2.6	3222 ± 1.0	0.2873 ± 0.0001	150.5 ± 0.1
1250-4	X	5902 ± 8.5	3222 ± 6.5	0.2877 ± 0.0004	150.4 ± 0.6
	Y	5901 ± 7.5	3224 ± 8.2	0.2872 ± 0.0008	150.7 ± 0.8
	Z	5899 ± 4.6	3224 ± 2.0	0.2870 ± 0.0001	150.7 ± 0.2
1250-6	X	5903 ± 7.5	3223 ± 5.0	0.2876 ± 0.0002	150.5 ± 0.5
	Y	5904 ± 4.5	3223 ± 4.5	0.2877 ± 0.0004	150.5 ± 0.5
	Z	5897 ± 6.1	3223 ± 3.1	0.2870 ± 0.0001	150.6 ± 0.3

5 Three-point bending test

To validate the elastic modulus values obtained from ultrasonic testing, static three-point bending tests were conducted. Specimens had a rectangular cross-section of 4 × 3 mm and were tested at a support span of 40 mm. A loading rate of 10 MPa/s was used, and measurements were performed on a Zwick/Roell Z005 universal testing machine.

It is important to recognize that bending modulus and ultrasonic modulus do not represent identical mechanical responses. Bending induces combined tensile and compressive stresses—analogous to the propagation mechanism of longitudinal ultrasonic waves—whereas transverse ultrasonic waves correspond to shear deformation.

Two testing procedures were used:

- Elastic-range loading (0–200 MPa) - Modulus derived from secant modulus, tangent modulus, chord/regression modulus and hysteresis modulus (from cyclic loading between 30–180 MPa).

  Cyclic preloading to partially exhaust plasticity - Each specimen was cycled 30× between 0–70 MPa before modulus determination. This method typically yielded slightly higher flexural modulus values. The lowest average moduli appeared in samples 1250-4, while the highest were found in 1000-2 samples.

Tab. 3 *Flexural modulus determined by static three-point bending test after HIP*

Sample no.	Direction	Flexural modulus [GPa] / first method	Flexural modulus [GPa] / second method (cycled samples)
1000 Ar	X	147.9 ± 3.25	148.4 ± 4.56
	Y	153.9 ± 6.10	151.8 ± 7,33
1000-2	X	151.4 ± 2.71	149.4 ± 7.27
	Y	150.2 ± 2.65	151.8 ± 6.52
1250 Ar	X	147.5 ± 4.93	150.9 ± 2.21
	Y	147.4 ± 3.20	147.5 ± 6.31
1250-4	X	135.7 ± 8.84	142.0 ± 5.12
	Y	132.7 ± 5.26	141.6 ± 6.17
1250-6	X	142.1 ± 4.40	143.4 ± 4.22
	Y	144.1 ± 4.42	147.6 ± 4,86

6 EBSD Analysis and Determination of Young's Modulus

6.1 Sample Preparation and Experimental Setup

Samples were extracted in two perpendicular orientations. The first group was taken in the Z–X direction and the second in the Y–X direction. After sectioning, all evaluated surfaces were prepared using standard metallographic procedures. Grinding was performed using SiC abrasive foils with grit sizes from P220 to P4000, followed by polishing on MD-Nap cloths with diamond suspensions of 1–3 μm. Final polishing was carried out with OP-U colloidal silica (0.04 μm) on MD-Nap cloths to ensure a deformation-free surface suitable for EBSD analysis.

For EBSD acquisition, the samples were mounted in a holder at a 70° tilt angle. Measurements were performed using a Tescan Mira 3 scanning electron microscope equipped with a NordlysNano EBSD detector. A secondary electron detector was used simultaneously. The working distance was 20–25 mm, the field of view 150 μm, and the accelerating voltage 15 kV. The detector was operated in 8×8 binning mode, with a step size of 0.294 μm. EBSD patterns were collected using Oxford Aztec software, and post-processing and crystallographic evaluation were performed in Aztec Crystal v3.1.

To determine Young's modulus, the single-crystal elastic constants were calculated. These were derived from ultrasonic wave velocities measured in the earlier UT analysis using equations (3–5) [6-9]:

Elastic stiffness constants:

$$C_{11} = \rho \cdot v_l^2 \tag{3}$$

$$C_{44} = \rho \cdot v_t^2 \tag{4}$$

Zener Elastic Anisotropy:

$$A = \frac{2 \cdot C_{44}}{C_{11} - C_{12}} \tag{5}$$

Where:

ϱ…Material density (kg/m³);

v_L, v_T…Longitudinal and transverse wave velocities (m/s);

A…Zener anisotropy (dimensionless).

Based on these relationships, the elastic stiffness constants C11, C12, and C44 for the ferritic phase present after heat treatment were calculated. Their values are summarised in Table 4 (units in $\times 10^{11}$ N/m²).

Tab. 4 *Elastic stiffness coefficients for a-ferrite phase*

Sample	Orientation	C11	C12	C44
1000-Ar	Z-X	2.723	0.815	2.044
	Y-X	2.727	0.813	2.049
1000-2	Z-X	2.731	0.815	2.052
	Y-X	2.733	0.815	2.054
1250-Ar	Z-X	2.725	0.815	2.046
	Y-X	2.728	0.814	2.050
1250-4	Z-X	2.732	0.816	2.052
	Y-X	2.734	0.815	2.054
1250-6	Z-X	2.730	0.815	2.050
	Y-X	2.736	0.815	2.056

6.2 Experimental Results

Table 5 presents the values of Young's modulus calculated using the Voigt, Reuss, Hill, and geometric mean approaches. The results show that the difference in Young's modulus between the Z–X and Y–X orientations is very small, with an average deviation of 2.5 ± 1.2 GPa.

When comparing individual material variants, the Young's modulus differed on average by:

- 6.3 ± 0.2 GPa in the Z–X orientation
- 8.9 ± 0.3 GPa in the Y–X orientation

The lowest Young's modulus was found in the 1000-Ar samples, while the highest was observed in the 1250-6 samples.

These results indicate that both printing parameters (laser power, shielding gas) and powder atomization method significantly influence the microstructural stiffness of the printed A508 steel.

Tab. 5 *Calculated elastic stiffness coefficients (ESC variant no. 4)*

Sample	Orientation	Voigt (GPa)	Reuss (GPa)	Hill (GPa)	Geometric (GPa)
1000-Ar	Z-X	171.1±4.2	145.6±4.4	158.4±4.3	160.3±4.4
	Y-X	169.2±2.5	143.7±2.6	156.5±2.5	157.9±2.5
1000-2	Z-X	170.1±5.0	145.4±5.8	157.8±5.4	159.2±5.7
	Y-X	175.2±4.6	151.1±5.1	163.2±4.8	165.1±5.1
1250-Ar	Z-X	172.9±3.3	148.2±4.6	160.6±3.9	162.1±4.1
	Y-X	174.8±0.73	150.1±0.8	162.4±0.7	164.2±0.8
1250-4	Z-X	175.8±1.1	150.9±1.3	163.4±1.2	165.2±1.2
	Y-X	174.1±1.3	149.2±1.4	161.7±1.3	163.3±1.4
1250-6	Z-X	176.2±0.6	151.6±0.5	164±0.5	166±0.6
	Y-X	177.5±2.5	152.8±2.8	165.2±2.6	167.3±2.8

The difference between the Young's modulus values obtained by EBSD and those determined by the other techniques arises primarily from the mathematical models used to estimate the polycrystalline elastic constants. These models rely on averaging schemes applied to the single-crystal elastic stiffness coefficients, and the choice of averaging method (Voigt, Reuss, Hill, or geometric mean) inherently leads to variations in the predicted modulus.

Another contributing factor is the significantly smaller analyzed volume in EBSD compared to the volumes evaluated by ultrasonic testing and three-point bending. EBSD probes only a surface-near region within a limited field of view, whereas UT methods and mechanical testing sample much larger material volumes. Consequently, local heterogeneities, microstructural gradients, or residual strain variations in the thermally affected regions may influence the EBSD-derived Young's modulus and contribute to the observed differences between methods.

7 Summary

From the UT perspective, the measured printing direction affects the final E values. The results of the elastic moduli in the Y axis, obtained by Pulse-Echo ultrasonic technique, the three-point flexural test using cycled specimens and EBSD analysis, are compared in Table 7.

Tab. 7 *Comparison modulus of elasticity in the Y axis measured by UT, 3-point bending test and EBSD*

Sample no.	1000-Ar	1000-2	1250-Ar	1250-4	1250-6
UT	150.1 ± 0.5	150.5 ± 0.4	150.2 ± 1.0	150.7 ± 0.8	150.5 ± 0.5
3-point bending	151.8 ± 7.3	151.8 ± 6.5	147.5 ± 6.3	141.6 ± 6.2	147.6 ± 4.9
EBSD (Hill)	143.7 ± 2.6	151.1 ± 5.1	150.1 ± 0.8	149.2 ± 1.4	152.8 ± 2.8

Across all materials, the values obtained by the ultrasonic method (UT) range from 145.4 to 150.2 GPa, showing a relatively narrow scatter and confirming good homogeneity of the printed and HIP-treated structures in the Y direction. The three-point bending test showed slightly higher variability (141.6–151.8 GPa), which is consistent with the fact that flexural loading is sensitive to small

differences in surface condition, machining quality and local bending stiffness. The EBSD-based Young's modulus exhibits a wider range (143.7–152.8 GPa), reflecting the effect of microstructural heterogeneity within the small analyzed volume.

Quantitative comparison (Table.8) of the methods showed good agreement. The average deviation between ultrasonic testing and the three-point bending method was 3.3 %, while the average deviation between ultrasonic testing and EBSD was 1.7 % (Reuss) and 6.7 % (Hill). These results confirm that all three approaches provide mutually consistent estimates of the elastic modulus of HIP-treated DED-printed A508 steel.

Tab. 8 *Percentage relative differences of the modulus of elasticity in the X-axis and Y-axis direction determined using UT, 3-point bending test (values form two testing procedures), and EBSD methods (values from the UT method as reference)*

	1000-Ar		1000-2		1250-Ar		1250-4		1250-6	
UT-three-point bending test [%]	X-axis	Y-axis	X-axis	Y-axis	X-axis	Y-axis	X-axis	Y-axis	X-axis	Y-axis
	1.45	1.80	0.01	0.33	0.80	1.87	8.32	9.88	5.43	3.19
UT-EBSD (Reuss) – [%]	X-axis	Y-axis	X-axis	Y-axis	X-axis	Y-axis	X-axis	Y-axis	X-axis	Y-axis
	3.23	4.45	3.37	0.40	1.48	0.07	0.33	1.01	0.73	1.51
UT-EBSD (Hill) – [%]	X-axis	Y-axis	X-axis	Y-axis	X-axis	Y-axis	X-axis	Y-axis	X-axis	Y-axis
	5.11	4.09	4.75	7.78	6.35	7.51	7.96	6.80	8.23	8.90

A paired two-tailed Student's t-test was used to compare the elastic modulus values obtained by the different methods. A comparison of the results from the static bending test and the UT method showed that the differences were not statistically significant for the 1000-Ar, 1000-2 and 1250-Ar samples. Both methods therefore provide consistent results and capture similar mechanical behavior of the material. However, the situation is different for the 1250-4 and 1250-6 samples. Here, the differences between bending test and UT become statistically significant, which corresponds to significant changes in the microstructure. The mechanical response during three-point bending test is more sensitive to these changes than ultrasound, which measures the effective modulus via the propagation of elastic waves. The Reuss model, which represents minimum stiffness (orientations loaded in accordance with the softest crystallographic directions), shows statistically insignificant differences compared to the UT method in all samples. The Hill model, which is an average of the Reuss and Voigt models, provides elastic modulus values that are statistically significantly higher than the UT measurements in all samples.

When comparing individual materials, the highest elastic modulus in two methods was consistently identified in the 1250-6 samples, while the lowest values were found in the 1000-Ar material. This trend is visible across UT, bending and EBSD and indicates a systematic influence of the printing parameters (laser power and shielding gas) on the resulting elastic stiffness after HIP treatment.

Because EBSD evaluates only a shallow, locally confined region, its values are more sensitive to local texture, grain orientation, or residual stresses. In contrast, ultrasonic and mechanical testing integrate significantly larger volumes; therefore, EBSD may deviate more strongly when microstructural gradients or local anisotropy are present. Nevertheless, the applied averaging models (Reuss and Hill) provide EBSD-based moduli that are generally consistent with UT and mechanical test data for all material variants.

The overall comparison demonstrates that the non-destructive Pulse-Echo ultrasonic technique provides reliable results, closely matching those from destructive three-point bending tests. Consistency between the two methods is ensured when the mechanical test specimens are oriented in the same direction as the propagation of the ultrasonic waves used in UT and when the specimens do not have a significantly altered structure [2, 5]. Accurate thickness calibration using 3D scanning significantly contributed to reducing uncertainty in wave velocity determination and enabled close agreement with mechanical results.

Taken together, the findings confirm that equations (1) and (2) based on longitudinal and transverse ultrasonic velocities (c_l and c_t) are suitable and accurate for determining the elastic modulus of DED-printed and HIP-processed materials. Ensuring stable measurement conditions, particularly constant coupling medium and probe pressure, is essential to achieve reproducible ultrasonic results and to maintain consistency with mechanical and EBSD-based evaluations.

Although the overall variation of Young's modulus among the investigated material variants was relatively small, systematic differences were observed between individual printing conditions. The results indicate that laser power and powder atomization conditions influence the resulting elastic stiffness even after HIP processing.

The presented conclusions are based on A508 steel produced by DED technology after HIP treatment. Further work will focus on extending the methodology to other additively manufactured alloys and on correlating elastic modulus with porozity, texture and residual stress distributions.

Acknowledgement

The presented work has been realized within Institutional Support by Ministry of Industry and Trade of the Czech Republic.

References

[1] ÁLVARO, B.D.C.J., MARIA HELENA, T. L., MAURÍLIO, J. I, SAMARA, G.R., DEBORA, S.R., GUSTAVO, D. F., VINÍCIUS, M.B.F., JAIRO, A.V.D.O. (2022). Determination of elastic and mechanical properties in CA-50 steel by using ultrasonic waves. *International Journal of Advanced Engineering Research*, Vol.9, Issue 9, https://dx.doi.org/10.22161/ijaers.99.25.

[2] R. HASAN, A. F. ABU SAMAH, AND Z. SHAMSUDIN, (2024). Comparison of Young's Modulus determination from Ultrasonic Testing and Three-Point Bending Testing", *J. Adv. Res. Appl. Mech.*, vol. 121, no. 1, pp. 58–65, https://doi.org/10.37934/aram.121.1.5865.

[3] OLYMPUS / Evident, In: *Elastic Modulus Measurement*. 2002.

[4] NANEKAR, P.P., SHAH, B.K., (2003). Characterization of material properties by ultrasonic. *BARC Newsletter*, vol. Issue No. 249.

[5] STEPANOV, S.I., ZORINA, M.A., SATSKII, D.D., KARABANALOV, M.S., PUZANOV, M.P., LOGINOV, Y.N., LOBANOV, M.L. (2026). Estimation of elastic modulus anisotropy in grain-oriented electrical steel using EBSD and DMA methods. *Lett. Mater.*, 16(1) 71-77, https://doi.org/10.48612/letters/2026-1-71-77.

[6] LEDBETTER, H.M., (1984). Monocrystal-polycrystal elastic constants of a stainless steel, *Physica Status Solidi (a)*, 85(1), pp. 89–96. doi:10.1002/pssa.2210850111.

[7] SHAWISH, E.S. et al. (2021) 'IA single grain boundary parameter to characterize normal stress fluctuations in materials with elastic cubic grains', *European Journal of Mechanics- A/Solids*.

[8] BODA, R., PANDA, B., KUMAR, S. (2024) 'Bioinspired design of isotropic lattices with tunable and controllable anisotropy', *Advanced Engineering Materials* [Preprint]. doi:10.1002/adem.202401881.

[9] TEKLU, A. *et al.*, (2004). Single-Crystal Elastic Constants of fe-15ni-15cr alloy, *Metallurgical and Materials Transactions A*, 35(10), pp. 3149–3154. doi:10.1007/s11661-004-0059-y.

[10] VESELÁ, J., P. BENEŠ and D. BRICÍN. Effect of Thermal Ageing on Changes in Modulus of Elasticity E Measured by Ultrasound, Bending Test and EBSD. *Manufacturing Technology*. 2025, Vol. 25, No. 3. DOI: 10.21062/mft.2025.038.

[11] HÜRLOVÁ H., DALIBOR V. Microstructure and Mechanical Properties of Biomedical Co-Cr-Mo Alloy Produced by Precision Casting and 3D Printing Technologies. *Manufacturing Technology*. 2026, 26(2), 1–8. DOI: 10.21062/mft.2026.013.

[12] CHLUPOVÁ, ALICE, JAKUB POLOPRUDSKÝ, MICHAL JAMBOR, JAROMÍR BRŮŽA, LADISLAV POCZKLÁN A JIŘÍ MAN. Heat Treatment-Induced Microstructural Changes in Selectively Laser Melted AlSi10Mg Alloy. *Manufacturing Technology*. 2025, 25(6). DOI: 10.21062/mft.2025.077.

[13] SIREGAR, I. et al. Milling Performance of Selective Laser Melted Ti6Al4V: A Taguchi Approach for Surface Roughness Optimization. *Manufacturing Technology*. 2025. DOI: 10.21062/mft.2025.030.

[14] CZAN, A. et al. Analysis of the Basic Characteristics of the Working Accuracy of the Atomic Diffusion Additive Manufacturing ADAM Process by Comparison with the Selective Laser Melting SLM Process. *Manufacturing Technology*. 2024. DOI: 10.21062/mft.2024.015.